Eur. Phys. J. B **13**, 87–97 (2000)

THE EUROPEAN PHYSICAL JOURNAL B

EDP Sciences

Spectral properties of incommensurate charge-density wave systems

G. Seibold[1], F. Becca[2], F. Bucci[2], C. Castellani[2], C. Di Castro[2], and M. Grilli[2,a]

[1] Institut für Physik, BTU Cottbus, PBox 101344, 03013 Cottbus, Germany
[2] Istituto Nazionale di Fisica della Materia e Dipartimento di Fisica, Università di Roma "La Sapienza", Piazzale A. Moro 2, 00185 Roma, Italy

Received 14 June 1999

Abstract. The concept of frustrated phase separation is applied to investigate its consequences for the electronic structure of the high T_c cuprates. The resulting incommensurate charge density wave (CDW) scattering is most effective in creating local gaps in k-space when the scattering vector connects states with equal energy. Starting from an open Fermi surface we find that the resulting CDW is oriented along the (10)- and (or) (01)-direction which allows for a purely one-dimensional or a two-dimensional "eggbox type" charge modulation. In both cases the van Hove singularities are substantially enhanced, and the spectral weight of Fermi surface states near the M-points, tends to be suppressed. Remarkably, a leading edge gap arises near these points, which, in the eggbox case, leaves finite arcs of the Fermi surface gapless. We discuss our results with repect to possible consequences for photoemission experiments.

PACS. 74.72.-h High-T_c compounds – 74.25.-q General properties; correlations between physical properties in normal and superconducting states

1 Introduction

Striped phases are an important issue in the discussion on physical properties of the high-T_c materials [1,2]. Incommensurate magnetic peaks displaced from the antiferromagnetic wave-vector along $\mathbf{k}_x$ and $\mathbf{k}_y$ have been observed by inelastic neutron scattering in both $La_{2-x}Sr_xCuO_4$ [3–5] and $YBa_2Cu_3O_{7-x}$ (YBCO) [6], whereas in the $Bi_2Sr_2CaCu_2O_8$ material the incommensurate magnetic peak position has not yet been resolved [7]. However, incommensurate magnetic scattering may result from either some kind of spiral phase (involving a modulation of the transversal spin components only) or from longitudinal spin fluctuations where in this case a strong coupling to the charge is expected. Evidence for cooperative charge- and spin scattering is based on the observation of domain walls in $La_{1.6-x}Nd_{0.4}Sr_xCuO_4$ [8] where the low temperature tetragonal lattice structure and the filling close to 1/8 are suited to pin the density fluctuations, giving rise to a static CDW phase as revealed by commensurate ionic shifts observed in neutron scattering. From the temperature dependence of the charge- and spin-order peaks one can further conclude that the stripe order is driven by the charge rather than by the spins. Additional support for charge induced stripe correlations is provided by recent neutron scattering studies of the phonon dispersion in YBCO [9]. These measurements show a large broadening in the spectrum at wave vectors which are twice the magnetic incommensurability. Moreover, the broadening in the phonon spectrum occurs at higher temperatures than the incommensurable magnetic peaks indicating again that charge fluctuations are the "driving force" behind incommensurable magnetic scattering.

The formation of stripe correlations in these compounds can be well understood within the concept of frustrated phase separation [10] where a phase separation instability is prevented by long-range Coulomb interactions [11]. As a result the long-wavelength density fluctuations associated with phase separation are suppressed in favor of shorter-wavelength density fluctuations, giving rise either to dynamical slow density modes [10] or to incommensurate charge density waves (CDW) [1,12]. Concerning the pairing mechanism the theoretical proposals differ with regard to the role of the stripe correlations on the superconducting pair formation. Whereas some theories consider the formation of quasi 1-d "rivers of charge" as a necessary environment for the quasiparticles to pair or to enhance T_c [2,13] others take the fluctuations associated with the stripe instability itself as a pairing mechanism [1].

The proximity to a stripe instability tuned by doping and temperature allows to interpret many properties of the cuprates as due to a Quantum Critical Point (QCP) [14] located near optimal doping [1,15–17]. Within this scenario the singular scattering induced by the critical fluctuations would be responsible for both the anomalous

[a] e-mail: marco.grilli@roma1.infn.it

normal-state properties and the large superconducting critical temperatures. Then the phase diagram of the cuprates is partitioned in the (nearly) ordered, the quantum critical, and the quantum disordered regions corresponding to the under-, optimally, and over-doped regions of the phase diagram of the cuprates.

The relevance of the stripe phase and of the stripe fluctuations should find an experimental confirmation (or a disproof) in the analysis of the single-particle spectral properties. Taking the point of view that incommensurate CDW scattering contributes to determine the electronic properties of the high-T_c materials the question arises how the electronic structure around the Fermi energy is affected by this scattering and if this can be detected by angle-resolved photoemission spectroscopy (ARPES) [18]. In fact, there are several features which seem to be common to all p-type cuprates (see *e.g.* Ref. [19] and references therein). In particular, the dispersion displays an extended saddle-point at $(\pi/a, 0)$ (where a is the lattice spacing) with an energy close to E_F, which has been observed in Bi2212 [20] as well as in YBaCuO [21] samples. Furthermore, the Fermi surface of Bi2212 is very strongly nested with a nesting vector of approximately 0.9 $(\pi/a, \pi/a)$. The resulting picture for the Fermi surface therefore consists of tube-like structures around the M-points which are connected by more or less straight pieces. It has been shown in reference [22] that many of these unusual Fermi surface features can be explained by assuming a disordered stripe phase to be present in the high-T_c copper oxides. The fact that the charge carriers are exposed to a stripe potential mirrors in the Fermi surface through one-dimensional characteristics which predominantly appear around the M-points.

A further fascinating Fermi surface feature of the high T_c superconductors, which has been detected in ARPES measurements concerns the pseudogap phenomenon which is observed in optimally and underdoped bismuth compounds below a doping dependent temperature $T^* > T_c$ [23–26]. In underdoped samples of Bi2212 [23,24] there is a qualitative change in the electronic structure with respect to the optimally doped system already above T_c, with the appearance of so-called leading-edge gaps around the M points. In these k-space regions there is no indication of a quasiparticle peak, and the spectra are dramatically broadened and shifted to higher binding energies with a maximum at 100–200 meV. As a consequence large portions of the Fermi surface around these points are not visible whereas along the $\Gamma \rightarrow X$ directions the spectral lineshapes are similar to those of the optimally doped samples. Similar results where obtained in the one-plane material Bi2201 [25] showing that bilayers are not essential to the pseudogap phenomena.

A common explanation for the features described above is based on the existence of pre-formed pairs already above T_c, since a continuous evolution of the spectra from the normal to the superconducting state [27] was apparently observed. In particular, a superconducting d-wave gap is in accordance with the symmetry of the pseudogap. Moreover, for materials with $k_F\xi_0 < 10$ the existence of two temperature scales for pairing and phase coherence is a rather natural consequence. However, this simple scenario is put in jeopardy by various experimental findings. First of all the rapid increase of T^* by decreasing doping is to be contrasted with the much more moderate increase of the maximum gap at low temperature. (T^* doubles when T_c goes from 90 K to about 75 K in Bi-2212, whereas in the same doping range, $\Delta(T = 0)$ around the M-points changes by thirty per cent at most.) This suggests that a substantial temperature dependence of the pairing potential is present in this doping range. Furthermore recent ARPES experiments [28] show that the pseudogap above T_c gradually appears at the M points leaving extended segments of the Fermi surface gapless. These segments continuously shrink to a point-like node only below the superconducting critical temperature T_c. Needless to say that these behaviors do not correspond neither to the usual BCS gap opening process nor to the phase locking of uniform preformed pairs. Instead it might find an interpretation along the line of coexisting pairs and fermionic quasiparticles [29,30].

In front of this unsettled issue, one may ask whether the rich and unexplained behavior of the pseudogap phenomena could result from an electron-hole pair scattering above T_c rather than from pair correlations alone. This line of argumentation has been followed in several analyses based on the scattering between fermions and collective spin excitations [31–33]. A quite similar outcome would instead arise from the quasiparticles being scattered by incommensurate charge fluctuations [34]. The fact that a substantial part of the spectral features of the optimally and underdoped cuprates can be explained in terms of particle-hole scattering is also supported by recent experiments [26] measuring the Fermi surface by sequential angle-scanning photoemission. These results clearly show the missing segments of the Fermi surface around the M-points with a shape, which can be interpreted in terms of scattering of the quasiparticles with quasicritical mixed spin and charge fluctuations [34].

The idea that the pseudogap could (not only) arise from pairing in the particle-particle channel, but also from different scattering mechanims (like CDW fluctuations) finds an additional support in the recent analysis of reference [35], where the experimental results on the low-temperature penetration depth suggest that the doping behavior of the low-temperature gap near the nodes in the (1,1) direction is similar to what expected from standard d-wave BCS theory with the gap scaling with T_c. This is in contrast with the behavior of the pseudogap measured at the k-points around $(\pm\pi/a, 0)$ and $(0, \pm\pi/a)$ in ARPES experiments below T^*, which increases with decreasing T_c. This suggests the possibility that at high temperature ($T^* > T > T_c$) the gap is due to CDW fluctuations scattering in the particle-hole channel. In this regard it was shown in references [1,12] that the incommensurate CDW scattering resulting from the competition between phase separation and long range repulsive Coulomb forces, occurs near some scattering vector $\mathbf{q}_c$ not related to the Fermi vector k_F. It was also shown within a standard large-N approach [1,12] that the effective scattering amplitude close to $\mathbf{q}_c$ in the particle-hole channel is

strongly attractive and similarly structured in momentum space in the particle-particle channel also, thus resulting in substantial pairing in the d-wave channel. Within this scenario, the strong momentum-dependent effective interaction is responsible both for (preformed) pairing and for pseudogap formation due to dynamical charge modulation. Therefore searching for spectral features arising from scattering mechanisms acting in the particle-hole channel is not necessarily in contrast with the interpretation of other features in terms of pairing in the particle-particle channel.

In the present paper we are interested in the question if incommensurate CDW scattering, resulting from the competition between phase separation and long range repulsive Coulomb forces, can account for some of the above anomalous features observed in photoemission experiments. This problem was partly tackled in reference [34] within a perturbative treatment of quasicritical spin and charge fluctuations. This perturbative approach is unfortunately not feasible in the underdoped region, deep inside the stripe phase. Therefore we perform here a mean-field analysis, which should capture the non-perturbative character of well-formed stripes. Of course, the dynamical character of the stripe fluctuations will be missed. Nevertheless, at short distances and time as those probed in photoemission experiments, this description should be appropriate.

We emphasize once again that the complexity of the physics of the cuprates, particularly of the underdoped ones, involves spin and Cooper as well as charge density fluctuations. Our aim is therefore *not* to account for all the spectral properties of these materials, which likely arise from the interplay of all these mechanisms. We rather conservatively aim to point out that some of the prominent (and puzzling) features of the cuprates could find a natural interpretation by assuming charge quasi-ordering.

The paper is structured as follows. In Section 2 the model and the general formalism are presented. Section 3 contains the physical results for the Fermi surface and the spectral densities, which are discussed and summarized in the conclusive Section 4.

2 Formalism

Starting point is the Hubbard-Holstein model with an additional in-plane long-range Coulomb interaction

$$\begin{aligned} H = & -t \sum_{\langle i,j\rangle,\sigma} (c^\dagger_{i\sigma} c_{j\sigma} + H.c.) \\ & - t' \sum_{\langle\langle i,j\rangle\rangle,\sigma} (c^\dagger_{i\sigma} c_{j\sigma} + H.c.) \\ & + g \sum_{i\sigma} (A^\dagger_i + A_i)(n_{i\sigma} - \langle n_{i\sigma}\rangle) \\ & + \omega_0 \sum_i A^\dagger_i A_i - \mu_0 \sum_{i\sigma} n_{i\sigma} + U \sum_i n_{i\uparrow} n_{i\downarrow} \\ & + \frac{1}{2} \sum_q \frac{V_\mathrm{c}}{\sqrt{G^2(q) - 1}} \rho_q \rho_{-q} \end{aligned} \tag{1}$$

where $c_{i\sigma}(c^\dagger_{i\sigma})$ destroys (creates) an electron with spin σ at site i and $A_i(A^\dagger_i)$ destroys (creates) a local Holstein-type phonon at site i. The summation over nearest- and next-nearest neighbour sites is indicated by $\langle i,j\rangle$ and $\langle\langle i,j\rangle\rangle$, respectively. $\sum_\sigma n_{i\sigma} = \sum_\sigma c^\dagger_{i\sigma} c_{i\sigma}$ is the local electron density and its Fourier transform is given by $\rho_q = \sum_{k\sigma} c^\dagger_{k+q\sigma} c_{k\sigma}$. The last term in equation (1) describes the Coulomb interaction between electrons on a two-dimensional, square lattice (lattice constant a in x- and y-direction), which is considered as a plane embedded in the 3-dimensional lattice (plane distance d in the z-direction). The dielectric constants in the plane and perpendicular to it are given by $\epsilon_\parallel$ and $\epsilon_\perp$, respectively. The Coulombic coupling constant is $V_\mathrm{c} = \frac{\mathrm{e}^2 d}{2\epsilon_\perp a^2}$. On the $z = 0$ plane the momentum dependence of the Coulomb potential is found to be $G(q_x, q_y) = [\epsilon_\parallel/\epsilon_\perp (a/d)^2][\cos(aq_x) + \cos(aq_y) - 2] - 1$. As usual, the sum in the Coulombic potential does not include the zero-momentum component, since we are supposing that the diverging $q = 0$ interaction between electrons is canceled by the contribution of a uniform positively charged ionic background.

Since we are interested in the limit of strong local repulsion, we take the limit $U \to \infty$, which gives rise to the local constraint of zero double occupancy $\sum_\sigma n_{i\sigma} \leq 1$. To implement this constraint we use a standard slave-boson technique [36,37] by performing the usual substitution $c^\dagger_{i\sigma} \to c^\dagger_{i\sigma} b_i$, $c_{i\sigma} \to c_{i\sigma} b^\dagger_i$ and implement the local constraint by a local Lagrange multiplier λ_i. The model can first be solved in the mean field approximation by setting the $b^{(\dagger)}_i$ and λ_i bosons to their constant self-consistent values b_0 and λ_0, respectively. At this stage the phonons and the Coulombic interaction decouple from the fermionic quasiparticles for an homogeneous mean-field solution. The system then results in free quasiparticles with a shifted chemical potential $\mu = \mu_0 - \lambda_0$ and a dispersion $E_k = -2tb_0^2\epsilon_k$, where $\epsilon_k = [\cos(ak_x) + \cos(ak_y] + t'/t[\cos(ak_x + ak_y) + \cos(ak_x - ak_y)]$ and $b_0^2 = \delta$ corresponds to the concentration of doped holes. The mean-field value for λ_0 is determined by $\lambda_0 \equiv \lambda_0^0 + (t'/t)\lambda_0^1 = 2t \sum_k f(E_k)\epsilon_k$ where $f(E)$ is the Fermi function.

The effective interaction leading to scattering between quasiparticles arises from the exchange of the bosonic fields beyond the mean-field approximation. Working within the radial gauge [37] one can define a three-component field $\alpha^\mu = (\delta r, \delta\lambda, \delta\phi)$ where $\delta\phi$ is the lattice displacement field, and δr, $\delta\lambda$ are the fluctuating parts of the modulus of the $b^{(\dagger)}_i$-bosons and of the Lagrange multiplier λ_i respectively. The static bare scattering amplitude in the particle-hole channel can be written as [12]

$$\Gamma_0(k, k'; q) = -\sum_{\mu\nu} \Lambda^\mu(k', -q) D_0^{\mu\nu}(q) \Lambda^\nu(k, q) \tag{2}$$

where the vertices Λ^μ coupling the fermionic quasiparticles to the bosons are defined as

$$\begin{aligned} \Lambda_r(k, q) &= -2tb_0^2(\epsilon_{k+q/2} + \epsilon_{k-q/2}) \\ \Lambda_\lambda(k, q) &= i \\ \Lambda_\phi(k, q) &= -2g \end{aligned}$$

and $D_0^{\mu\nu}(q)$ denotes the matrix of the bosonic Greens function [12] with the inverse having all elements zero

except for

$$\begin{aligned}[D_0]^{-1}_{r,r} &= \delta\big[\lambda^0_0[\sin^2(q_x a/2)+\sin^2(q_y a/2)] \\ &\quad + (t'/t)\lambda^1_0[\sin^2((q_x-q_y)a/2) \\ &\quad + \sin^2((q_x+q_y)a/2)]\big], \\ [D_0]^{-1}_{r,\lambda} &= [D_0]^{-1}_{\lambda,r} = i\delta, \\ [D_0]^{-1}_{\phi,\phi} &= 2\omega_0. \end{aligned} \tag{3}$$

We finally obtain a Hamiltonian, describing the effective interaction between quasiparticles

$$H = \sum_{k\sigma} E_k c^\dagger_{k\sigma} c_{k\sigma} + \frac{1}{2}\sum_q V_q \rho_q \rho_{-q} \tag{4}$$

where the static effective interaction is given by

$$\begin{aligned} V_q &= \Gamma(k_\mathrm{F}, k'_\mathrm{F}; q, \omega=0) \\ &= \tilde{U} + \gamma_q - \frac{2g^2}{\omega_0} + \frac{V_\mathrm{c}}{\sqrt{G^2(q)-1}} \quad \text{and} \\ \tilde{U} &= -4E_\mathrm{F}/\delta \\ \gamma_q &= \frac{\lambda^0_0}{\delta}[\sin^2(q_x a/2)+\sin^2(q_y a/2)] \\ &\quad + \frac{t'}{t}\frac{\lambda^1_0}{\delta}\big[\sin^2\big((q_x-q_y)a/2\big)+\sin^2((q_x+q_y)a/2)\big]. \end{aligned} \tag{5}$$

Within a Fermi-liquid scheme, V_q represents the effective residual interaction between the quasiparticles once the screening due to intraband particle-hole quasiparticle bubbles is disregarded.

The Hamiltonian (4) is the starting point of all further investigations. Its interaction consists of a part, $\tilde{U}+\gamma_q$, increasing with $|\mathbf{q}|$, which describes the residual scattering of the quasiparticles through the slave-bosons exchange. The superposition of the long-range Coulombic part causes the interaction to exhibit a minimum as a function of $\mathbf{q}$. The electron-phonon coupling $2g^2/\omega_0$ rigidly shifts the potential to lower values. This will induce an instability in the density-density response function at a critical value of $\mathbf{q}=\mathbf{q}_\mathrm{c}$ when $1+V_{\mathbf{q}_\mathrm{c}}\Pi(\mathbf{q}_\mathrm{c})=0$, where $\Pi(\mathbf{q})$ is the particle-hole fermionic bubble. This instability marks therefore a transition to an incommensurate CDW with scattering vector $\mathbf{q}_\mathrm{c}$ [38].

To proceed we will approximate the effective model equation (4) by a Hartree factorization and assume that the symmetry of the system is broken with respect to a given vector $\mathbf{q}_\mathrm{c}$ and its multiples. Notice that retardation effects arising from the frequency dependence of the total scattering amplitude have been neglected at this level. This mean-field treatment of equation (4) finds some justification in investigating static or low-energy properties of the quasiparticles close to the Fermi level, whereas this approximation is crude in the analysis of dynamical properties at frequencies, which are comparable with the typical energies of the exchanged boson.

In order to reproduce the "unperturbed" Fermi surface (*i.e.* of the overdoped system) of the Bi2212 compounds at optimal doping we take the hopping parameter t' to be $t'=-0.45t$, which leads to an open Fermi surface centered around $(\pm\pi/a, \pm\pi/a)$. It turns out that within a linear response approach as in reference [12], for this kind of bandstructure the CDW instability occurs first in the (1,0) or (and) (0,1) directions. In fact, a negative value of t' enhances the density of states around the M-points, which mirrors in an enhancement of the fermionic bubble $\Pi(\mathbf{q})$ in the (1,0) and (0,1) directions. Thus in a RPA-like treatment the divergence of the density-density response function preferably takes place for $\mathbf{q}=\mathbf{q}_\mathrm{c}$ in the $(1,0)$ or in the $(0,1)$ directions. Within a linear-response analysis, the instability is forced to occur at a given wavevector and the above arguments are in favor of the instability taking place with a modulation alternatively in the x or y direction described by the order parameter $\langle\rho_q\rangle^{1D} = \sum_n \langle\rho_q\rangle \delta_{q,nq_\mathrm{c}^{x/y}}$. However, a non-linear instability (as the one here described by a standard set of Hartree mean-field equations) can also occur simultaneously along both directions leading to a two-dimensional eggbox type modulation of the charge. In this case, the density expectation value is given by $\langle\rho_q\rangle^{\mathrm{egg}} = \sum_n \langle\rho_q\rangle[\delta_{q,nq_\mathrm{c}^x} + \delta_{q,nq_\mathrm{c}^y}]$.

Although we are now dealing with an effective one-particle Hamiltonian, it is clear that the system cannot be diagonalized for general incommensurate $\mathbf{q}_\mathrm{c}$ vectors. We therefore represent $\mathbf{q}_\mathrm{c}$ as

$$\mathbf{q}_\mathrm{c} = \frac{\pi}{a}\left(\frac{n_x}{m_x}; \frac{n_y}{m_y}\right) \tag{6}$$

which allows us to simulate the "incommensurability" by increasing the values for both n_i and m_i, respectively. Once the scattering term in equation (4) is decoupled *à la* Hartree, for each k-point in the reduced Brillouin Zone (BZ), the bare Bloch functions $\Psi_\mathbf{k}(n) \equiv \Psi(\mathbf{k}+n\mathbf{q}_\mathrm{c})$ with k-vector $\mathbf{k}, \mathbf{k}+\mathbf{q}_\mathrm{c}, \mathbf{k}+2\mathbf{q}_\mathrm{c}, \ldots, \mathbf{k}+n_{\max}\mathbf{q}_\mathrm{c}$, are mixed by the interaction. $n_{\max}$ depends on $\mathbf{q}_\mathrm{c}$ *via* the condition $\mathbf{k}+(n_{\max}+1)\mathbf{q}_\mathrm{c} = \mathbf{k}$. For each k-point, the Hamiltonian can be put in a matrix form, which can be diagonalized thus finding the linear transformation from the bare Bloch states $\Psi_\mathbf{k}(n)$ to the new eigenstates $\Psi_\mathbf{k}(n) = \sum_m a_\mathbf{k}(n,m)\Phi_\mathbf{k}(m)$. The system can be diagonalized numerically and the CDW order parameters $\chi_n = V_{nq_\mathrm{c}}\langle\rho_{nq_\mathrm{c}}\rangle$ are determined self consistently. Once self-consistency is reached, the eigenvalues $\tilde{E}_\mathbf{k}(m)$ give the band structure of the system.

The spectral function in the full BZ then consists of a ensemble of weighted delta-functions and is given by

$$A_{\mathbf{k}+n\mathbf{q}_\mathrm{c}}(\omega) = \sum_m a^2_\mathbf{k}(n,m)\delta\big(\omega - \tilde{E}_\mathbf{k}(m)\big). \tag{7}$$

It should be noticed that this approach maintains its full validity as long as the initial constraint of no double occupancy is satisfied. Therefore we will restrict in the following to the cases where the CDW order parameter is small enough that the local density never exceeds one, $\sum_\sigma n_{i,\sigma} \leq 1$.

3 Results

In this section we will discuss the bandstructure, Fermi surface and photoemission spectra resulting from either

1-d or eggbox type CDW scattering. For simplicity, in the following a planar cell of unitary length ($a = 1$) will be used. Since in the sytems with two CuO_2 layers per unit cell (as in Bi2212) different stripe orientations in different planes or also in different regions of the same plane may be realized, we consider also the case of superimposed (10)- and (01)-stripes. On the other hand the eggbox-solution, where the symmetry is broken in the x and y directions at the same time, can be regarded as a model for 1-d stripes fastly fluctuating between the (10)- and (01)-direction, while maintaining a fixed $|\mathbf{q}_c|$. Furthermore, having in mind the possibility of dynamical CDW scattering we also investigate averaged disordered realizations of an eggox charge modulation, where fluctuations in the absolute length of the scattering vector will be considered.

3.1 One-dimensional CDW phase

The results in this section supplement considerations in reference [22] where some effects of 1-d CDW scattering on the spectral properties were investigated. Here we analyze the consequences of CDW scattering on the bandstructure and, differently from reference [22], we start from an open Fermi surface (induced by a next-nearest neighbor hopping term t' as discussed in the previous section).

Figure 1 displays the calculated Fermi surface (FS) of a one-dimensional (1,0)-CDW for a parameter set close to the instability and doping $\delta = 0.2$. Parameters such that $\mathbf{q}_c \approx (\pi/4, 0)$ were chosen, corresponding to a charge modulation with a period of 8 planar unit cells (here and in the following we will consider a unitary lattice spacing, a=1). Since we diagonalize the system in a reduced BZ defined by the choice of $\mathbf{q}_c$ in equation (6) the defolding of the bands leads to a redistribution of spectral weight for the FS states. The photoemission intensity for each k-point is given by the following integration over an energy window around the Fermi energy $I_k = \int_{E_F-\epsilon}^{E_F+\epsilon} d\omega f(\omega) A_{\mathbf{k}}(\omega)$ where $f(\omega)$ denotes the Fermi function and $A_{\mathbf{k}}(\omega)$ is the spectral function defined in equation (7). For simplicity the intensity range is divided into three ranges for high ($I_k > 0.5$, full circles), intermediate ($0.1 < I_k < 0.5$, open circles) and low ($0.01 < I_k < 0.1$, dots) intensity.

Similar to the results of reference [22] there appear displaced shadow bands with low intensity which are due to q_c-scattering processes of the original FS states. However, since we started with an open Fermi surface (due to a quasi one-dimensional bandshape around $(\pi, 0), (0, \pi)$) the k-space regions around the M-points are strongly affected by the scattering. Moreover, there appears an asymmetry between these two areas since around the M-point the scattering is along the FS branches whereas at $\bar{M}$ it connects the branches centered around X and Y. As a consequence more k-states are reduced in intensity around $(\pi, 0)$ since the number of states with approximately the same energy that can be connected by $\mathbf{q}_c$ is larger than around $(0, \pi)$. To analyze the electronic structure in more detail we plot in Figure 2 the bands with weight larger than 1% in the interesting symmetry directions $\Gamma \to X$ and $M \to X$. The intensity range is divided in the same way as in Figure 1 and the same symbols are used. Moving along $\Gamma \to X$ (Fig. 2a) one observes a rich gap structure around Γ which diminishes upon approaching the FS crossing where besides the main band only the two weak shadow bands survive. The multiband features around Γ are due to the fact that at the bottom of the band its slope is small and therefore many states with similar energy can be connected by the CDW vector. Taking the cut along $M \to X$ (Fig. 2b), which is orthogonal to $\mathbf{q}_c$, one observes that the CDW has induced the formation of a second band which upon approaching X rapidly loses in intensity. On the other hand the band along the $\bar{M} \to X$ direction (Fig. 2c) displays a CDW gap at the FS crossing since this direction is parallel to $\mathbf{q}_c$ and the size of the scattering vector is of the same order than the FS branch separation at $(\pi, 0)$. In Figure 3 we show the energy distribution curves corresponding to the bandstructure cuts of Figure 2. Along the $\Gamma \to X$ direction (Fig. 3a) the gapped structure around Γ appears as a broad multipeaked feature which evolves into a single peak upon moving towards the X-point.

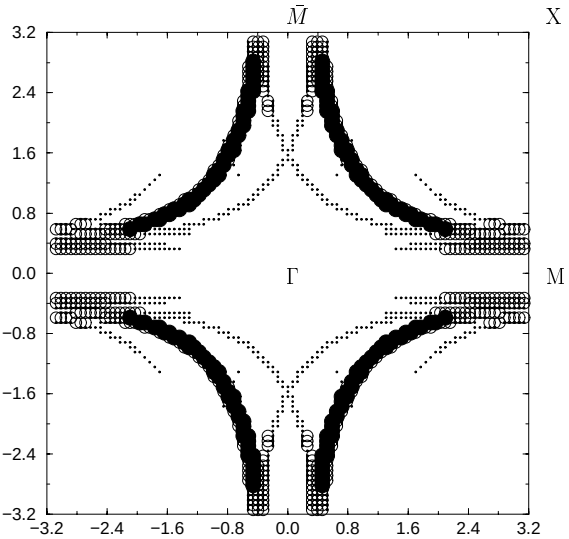

Fig. 1. Fermi surface for a 1-d charge modulation near the CDW instability where only the first harmonic $\chi_1 = 0.04$ is different from zero. Parameters: $\delta = 0.2$, $\alpha = -0.45$, $\omega_0 = 0.06$ eV, $g = 0.46$ eV, $V_c = 1.65$ eV. CDW modulation $|q_c| = 0.79$ in direction of $\Gamma - M$. The plot is for temperature $T = 100$ K and the energy window around E_F has choosen to be 50 meV. Intensities: $I > 50\%$: full points, $10\% < I < 50\%$: circles, $1\% < I < 10\%$: small dots.

For the cut along $M \to X$ one observes two peaks crossing the FS at $(\pi, 0.39)$ and $(\pi, 0.52)$ corresponding to the two bands in Figure 2b. The CDW along $\bar{M} \to X$ displays in a peak first moving towards the Fermi energy and then bending back to lower energies (Fig. 3c). However, this gap no longer can be detected when we consider a system with superimposed (10)- and (01) CDW scattering. The corresponding Fermi surface, bandstructure and energy distribution curves are plotted in Figures 2d, 3d and 4 respectively. Although there is still reduced weight

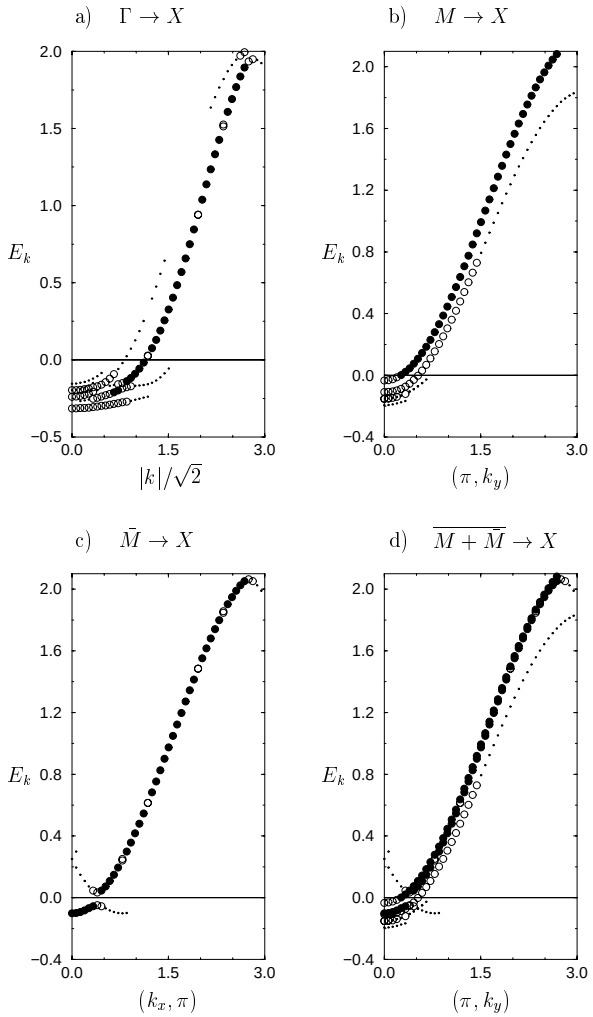

Fig. 2. (a-c): Cuts of the bandstructure in the full Brillouin zone along various symmetry directions for (10)-scattering, corresponding to the Fermi surface in Figure 1. (d): Superposition of the $M \to X$ and the $\bar{M} \to X$ cut, corresponding to the Fermi surface in Figure 1. Intensities: $I > 50\%$: full points, $10\% < I < 50\%$: circles, $1\% < I < 10\%$: small dots..

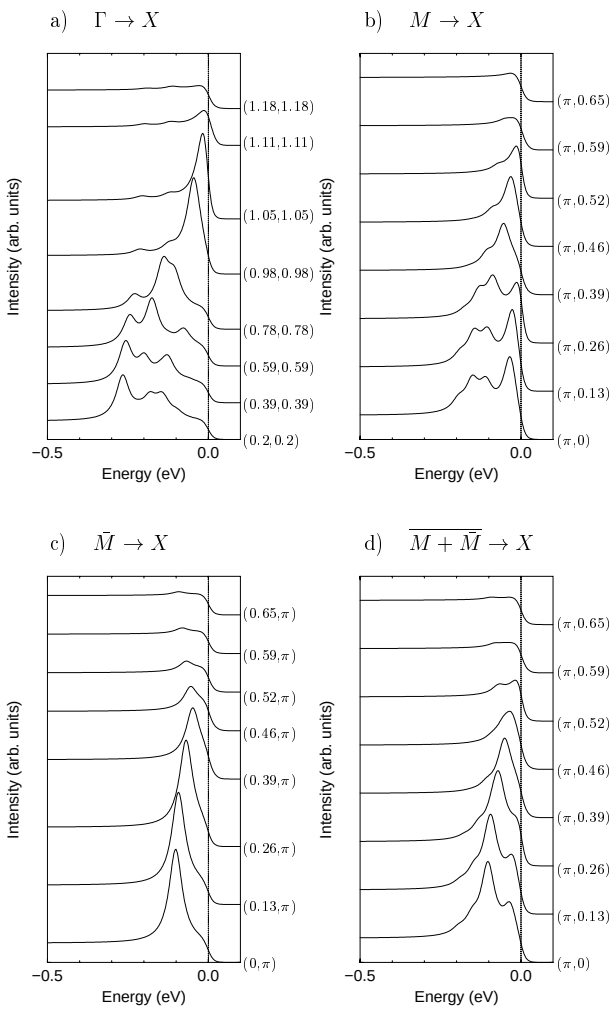

Fig. 3. Photoemission spectra corresponding to the cuts in Figure 3. The fermi function has been added as a background. The broadening of the δ-functions is 25 meV and the temperature $T = 100$ K.

of the k-states around $(0, \pi)$, $(\pi, 0)$, which are now equivalent, the CDW gap at $\bar{M}$ is no longer visible in Figure 3d since the averaged bandstructure is dominated by the states around the M-point.

It is also of interest to investigate the band dispersions along the $\Gamma \to M$ and $\Gamma \to \bar{M}$ directions. Along these directions a substantial enhancement of the van Hove singularities have been observed by ARPES experiments [18,20,21] and the obvious question arises whether this feature can arise from CDW scattering. Figure 5 reports in the (a) and (b) sectors the results of our calculation starting from an unperturbed bandstructure (indicated by the diamonds in Figs. 5a and 5b). It is apparent that multiple non-dispersive shadow bands appear along the $\Gamma \to M$ direction as a result of the CDW scattering, with a substantial redistribution of the spectral weight both at higher and lower energies. This latter occurrence suggests that indeed the broadening of quasiparticle spectra towards lower energies could experimentally be seen as a broadening in k-space of the area where the band is non-dispersive. For the presently considered (10) one-dimensional scattering, the same does not hold in the $\Gamma \to \bar{M}$ direction, where the shadow bands are strongly dispersive and much less numberous (Fig. 5b). As a consequence the spectra around $\bar{M}$ would hardly look like an enhanced van Hove singularity at low energy. However, the possibility still remains open that the spectra of the real materials can result from the (nearly static) superpositions of the spectra in Figure 5a, and 5b as a consequence of the different orientation of the stripes on different CuO_2 planes or on different regions of the same plane. This is depicted in Figure 5c. Alternatively, if the stripes are fastly fluctuating, their effect on the spectra could better be mimicked by our (static) eggbox solution described below.

3.2 Ordered eggbox phase

In this section we are concerned with a two-dimensional charge modulation resembling the shape of an eggbox.

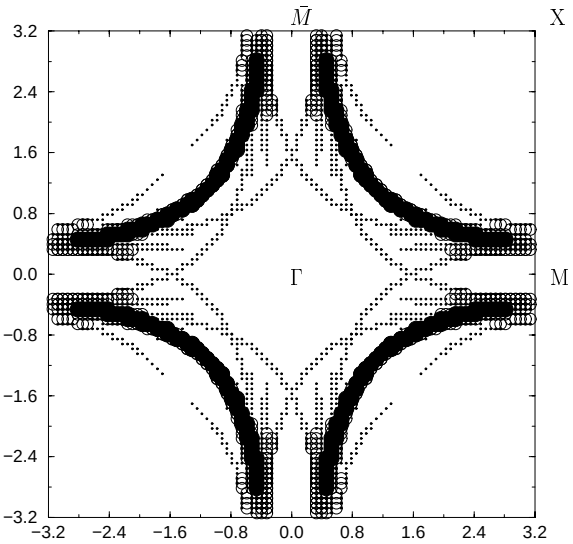

Fig. 4. Fermi surface for the superposition of the (10)-stripe of Figure 1 with the equivalent (01)-charge modulation. Parameters: $\delta = 0.2$, $\alpha = -0.45$, $\omega_0 = 0.06$ eV, $g = 0.46$ eV, $V_c = 1.65$ eV. CDW modulation $|q_c| = 0.79$. The plot is for temperature $T = 100$ K and the energy window around E_F has choosen to be 50 meV. Intensities: $I > 50\%$: full points, $10\% < I < 50\%$: circles, $1\% < I < 10\%$: small dots.

Figure 6 displays the calculated FS of a regular 2-d CDW for a parameter set close to the instability and doping $\delta = 0.2$. Similar to Figure 1 the scattering mostly affects the states around $(0, \pm\pi)$ and $(\pi, 0)$, but now of course the features at M and $\bar{M}$ are symmetric. Moreover, the region of reduced intensity is much larger than for the superimposed (01)- and (10)-CDW in Figure 4 (note that in both plots the strength of the order parameter is the same).

An additional quite interesting feature is the appearance of shadow Fermi surfaces in the $(1, \pm 1)$ directions, giving rise to "pockets". This feature was already hinted to in the Fermi surface of Figure 4, where it was, however less pronounced. In particular, here moving from the Γ point towards the X (or the other equivalent points) one first finds some spectral weight at the Fermi energy for points located around $(0.8, 0.8)$ in k-space. Moving further towards X one meets the main Fermi surface with highest intensity around $(1.2, 1.2)$, and then weak (less than 10% of intensity) features at $(1.6, 1.6)$. It is not unconceivable that these multiple crossings of the (shadow) Fermi surface(s) have been observed, although the common interpretation refers to magnetic scattering [32]. This finding suggests that, together with the magnetic scattering, charge scattering could cooperate to bring spectral weight at the Fermi surface in a "pocket-like" shape [34].

The effect of the 2-d scattering becomes more transparent in the bandstructure cuts plotted in Figure 7. Scanning along the diagonal direction gives a strong splitting of states around the Γ point similar to our previous findings for 1-d scattering. Moving further towards the X-point most of these states rapidly lose in intensity and at the FS crossing there is only one main band left together with

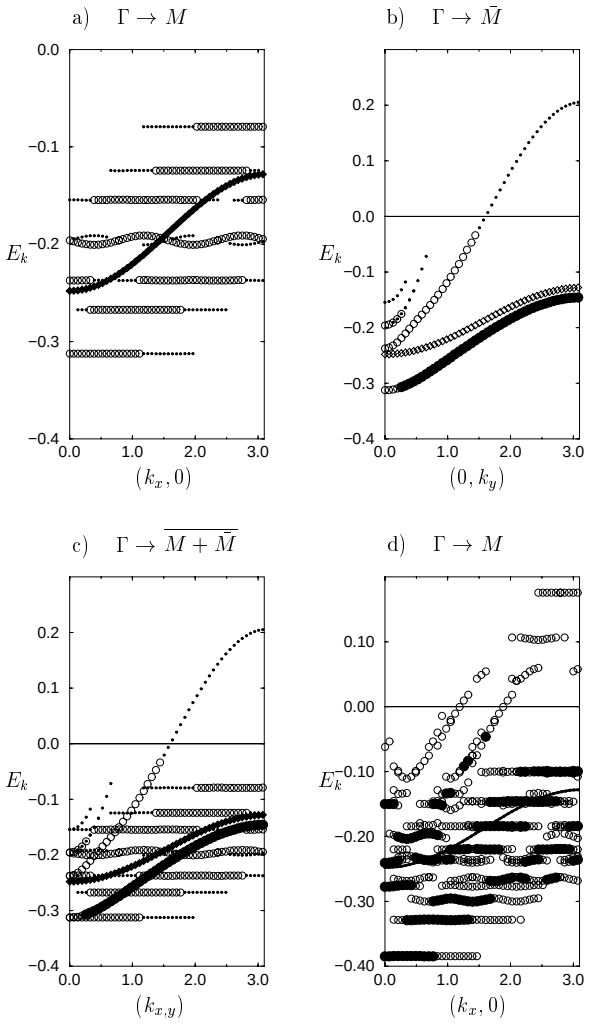

Fig. 5. (a-c) Bandstructure for one-dimensional CDW scattering along the (10)-direction for the same parameters as in Figure 1 of the paper. (a) $\Gamma \to M = (\pi, 0)$, (b) $\Gamma \to \bar{M} = (0, \pi)$, (c) Superposition of (a) and (b). The "unperturbed" band is indicated by diamonds. (d) The same cut for 2-d eggbox scattering. Here the "unperturbed" band is indicated by the full line. Intensities: $I > 50\%$: full points, $10\% < I < 50\%$: circles, $1\% < I < 10\%$: small dots.

two shadow bands with low intensity in accordance with the FS shown in Figure 6.

The band structure along $M \to X$ is plotted in Figure 7b. Also in this case we observe that at the M-point the CDW scattering has induced various bands with intermediate and low intensity. At the former FS crossing (indicated by the arrow) now a gap occurs which is of the order of the CDW order parameter χ. Although the main band (full circles) bends upwards when approaching the Fermi level there is a FS crossing by the shadow band with intermediate intensity. This crossing occurs at a slightly larger k_y value than in the unperturbed system which mirrors in Figure 6 as a broadening of the tube structure around the M-points.

In Figure 8 we show the energy distribution curves along the $\Gamma \to X$ and $M \to X$ directions. Scanning along

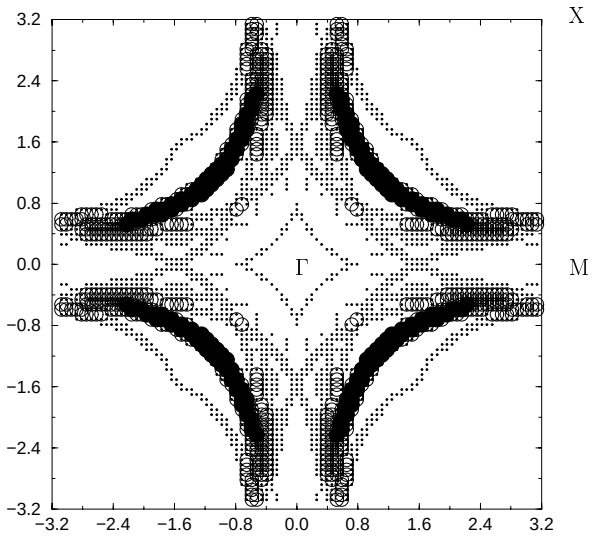

Fig. 6. Fermi surface for an eggbox type charge modulation near the CDW instability where only the first harmonic $\chi_1 = 0.04$ is different from zero. Parameters: $\delta = 0.2$, $\alpha = -0.45$, $\omega_0 = 0.06$ eV, $g = 0.46$ eV, $V_c = 1.65$ eV. CDW modulation $|q_c| = 0.79$. The plot is for temperature $T = 100$ K and the energy window around E_F has choosen to be 50 meV. Intensities: $I > 50\%$: full points, $10\% < I < 50\%$: circles, $1\% < I < 10\%$: small dots.

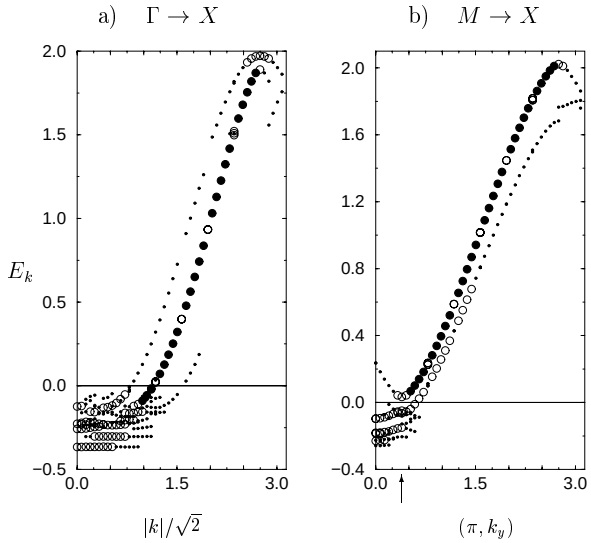

Fig. 7. Bandstructure in the full Brillouin zone corresponding to the Fermi surface in Figure 1. Intensities: $I > 50\%$: full points, $10\% < I < 50\%$: circles, $1\% < I < 10\%$: small dots. (a) $\Gamma \leq k \leq X$, (b) $M \leq k \leq X$.

the diagonal one clearly observes the multiple peak structure for the deeply bound states in Figure 7a. However, approaching the FS crossing, due to the rapid loss of intensity in the scattered bands, there appears a evolution into a single peak structure which crosses the Fermi level at $\mathbf{k} = (1.18, 1.18)$. In the right panel of Figure 8a we plot a comparison of the CDW spectra with the peak evolution of the homogeneous system for selected k-points. From this plot it becomes clear that along the diagonal direction the peak structure for the symmetry broken system

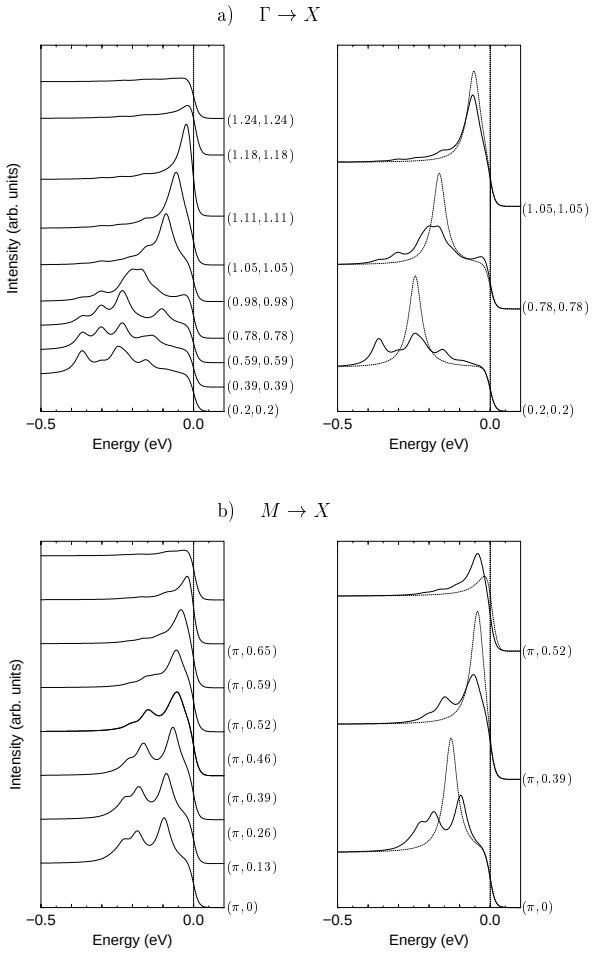

Fig. 8. Photoemission spectra for cuts along (a) $\Gamma \leq k \leq X$, (b) $M \leq k \leq X$. The fermi function has been added as a background. Solid lines: eggbox solution for the same parameter set as in Figure 1. Dashed lines: homogeneous system. The broadening of the δ-functions is 25 meV.

approaches the unperturbed form as one approaches E_F. On the other hand, scanning along the $M \to X$ direction, the peak structure basically is built up by the two bands with intermediate intensity below E_F which are shown in Figure 7b. Therefore one observes a double peak structure at the M-point where the lower peak decreases in intensity upon approaching the Fermi level. Due to the induced CDW-gap at the FS crossing of the homogeneous system $\mathbf{k} = (\pi, 0.52)$ there is a shift of the spectra to lower energy as can be seen from the right panel of Figure 8b. It is also quite interesting to see how the CDW-gap occurring at $\mathbf{k} = (\pi, 0.52)$ evolves when one moves along the FS of the unperturbed system. The corresponding energy distribution curves are shown in Figure 9. It turns out that the gap first keeps its value for small angles up to $\Theta \approx 6^o$. Moving towards the diagonal, the (pseudo)gap moves at energies below the Fermi level, so that at the Fermi energy it rapidly decreases and vanishes. This occurs at $\Theta \approx 20^o$. In addition it is again evident that upon approaching the diagonal direction the CDW peak structure evolves into the unperturbed one. These findings may correspond to the experimentally observed shrinking of the FS [28].

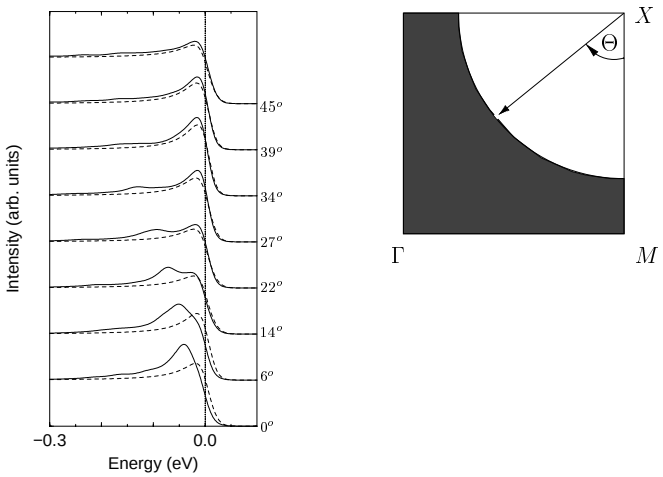

Fig. 9. Scan of the photoemission spectra along the unperturbed Fermi surface. The plots are labeled by Θ which is defined in the right panel. Full lines: CDW spectra; dashed lines: spectra of the unperturbed system.

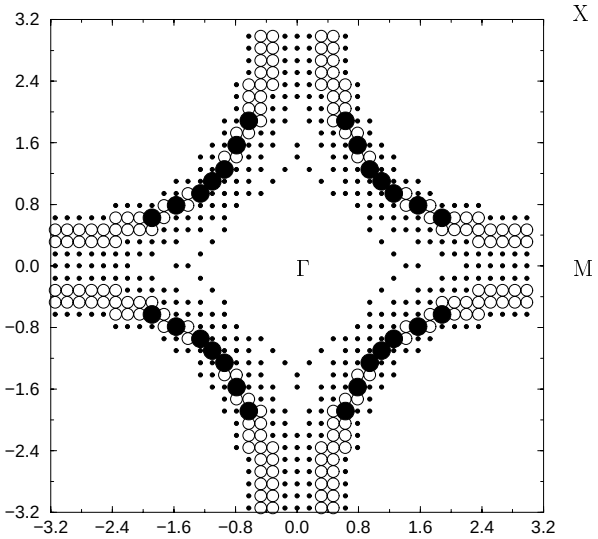

Fig. 10. Fermi surface for a disordered eggbox charge modulation. Parameters: $\delta = 0.2$, $\alpha = -0.45$, $p = 3$, $V_0 = 0.12$ eV. The plot is for temperature $T = 100$ K and the energy window around $E_{\rm F}$ has choosen to be 50 meV. Intensities: $I > 50\%$: full points, $10\% < I < 50\%$: circles, $1\% < I < 10\%$: small dots.

We now conclude this analysis of the 2-d eggbox CDW scattering by considering the relevant issue of the enhancement of the van Hove singularity around the M and $\bar{M}$ points. In particular, as it can be seen in Figure 5d, one finds a generic broadening of the spectra, with dispersionless portions of the spectrum scattered at both higher and lower energies with respect to the unperturbed quasiparticle band. Moreover, two dispersive shadow bands of weak intensity cross the Fermi energy nearly halfway between Γ and M. All these effects contribute to bring spectral weight at closer distance from the Fermi level. Once the spectral features observed in the present simplistic mean-field treatment are broadened by the fluctuative character of the CDW and by the many-body effects acting in the real systems, it is not unconceivable that our present findings correspond to an extension of the dispersionless region of the experimental band structure.

3.3 Disordered eggbox phase

In the preceding section we have considered an effective one-particle Hamiltonian so that all poles of the resulting spectral function correspond to delta functions. Now we want to extend our results to have some qualitative idea of a more dynamical description of the problem, *i.e.* the quasiparticle coupling to collective incommensurate CDW fluctuations.

As in reference [22] we start from a phenomenological one-particle Hamiltonian

$$H = \sum_k E_k n_k + \sum_i V(\mathbf{R}_i) n_i \tag{8}$$

where the kinetic part is the same as in the preceding section and $V(\mathbf{R}_i)$ represents an effective eggbox potential given by

$$V(\mathbf{R}_i) = 2V_0 \sum_n \mathrm{sech}\left(\frac{R_i^x - x_n}{\xi}\right) \mathrm{sech}\left(\frac{R_i^y - y_n}{\xi}\right). \tag{9}$$

The amplitude and broadening of the charge modulation is determined by V_0, ξ and x_n, y_n fix the positions of the individual "eggboxes". In accordance with the ordered eggbox modulation we choose a mean charge separation of $8a$ and define $x_{n+1} - x_n = y_{n+1} - y_n = 8a + \eta$ where "a" is the lattice constant and η is a random number varying between $-pa < \eta < pa$. Taking $p = 0$ one has again an ordered eggbox potential whereas upon increasing p ($p_{\max} = 7$) long-range charge order is destroyed to an increasing degree. The charge amplitude V_0 is restricted again to values where zero double occupancy at each lattice site is preserved. The results presented below are averages over five random configurations calculated by diagonalizing a square lattice with dimension 40×40 in real space. Doping is again $\delta = 0.2$ and the secans-type structure is broadened by $\xi = 2$.

Figure 10 displays the Fermi surface for a disordered eggbox-type charge modulation. The qualitative features are the same as in Figure 6, namely the reduction of intensity around the M-points. However, the displaced shadow bands are no longer visible now. Instead the Fermi surface is smeared in k-space *i.e.* its boundaries consist of states with low intensity ($< 10\%$). Around the M-points these states completely fill up the tube structure. This could correspond to the findings of sequential angle-scanning photoemission where diffuse features in these regions have been detected [26] and to the suppression of the FS observed in ARPES [28].

Since we are considering averages over disordered charge configurations the energy bands corresponding to

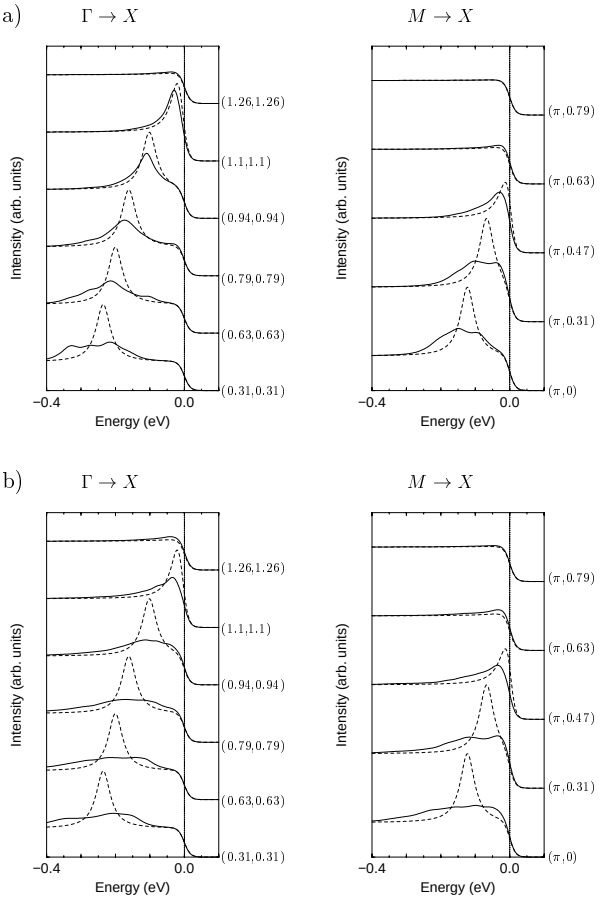

Fig. 11. Photoemission spectra for cuts along $\Gamma \leq k \leq X$ and $M \leq k \leq X$ for the same parameter set then in Figure 6. The broadening of the δ-functions is 25 meV. Dashed lines: homogeneous system. Solid lines: spectra for the disordered eggbox system. The parameter p defining the destruction of long-range charge order is $p = 3$ in (a) and $p = 7$ in (b).

Figure 7 now are also smeared along the energy axis therefore removing the fine structure of the CDW gap topology. This can be seen in Figure 11 where we have plotted the energy distribution curves along the $\Gamma \rightarrow X$ and $M \rightarrow X$ directions in comparison with the homogeneous system for two different values of the parameter p which defines the degree of suppression of long-range charge order. This smearing of the individual CDW peaks is of course more pronounced for $p = 7$ in Figure 11b than for $p = 3$ in Figure 11a. However, scanning along the $\Gamma \rightarrow X$ direction we observe the same feature than for the ordered eggbox modulation, namely the evolution of the spectra into a single peak structure upon approaching the Fermi level thus recovering the FS segment of the quasiparticle. On the contrary, at the M-point the quasiparticle peak is now completely suppressed and the spectra are described by a broad feature extending to very low energies.

4 Discussion and summary

In this paper we have investigated the possible consequences of incommensurate CDW scattering with regard to the unusual Fermi surface and photoemission features in underdoped bismuth cuprates already mentioned above. Our results have been obtained within a scheme, which is subjected to some limitations both at the level of the starting model and of its treatment. In particular, only the physics of CDW modulations has been considered, thus neglecting the relevant interplay between charge, spin, and Cooper pair fluctuations. Nevertheless it is quite interesting and instructive by itself that our treatment of a pure CDW symmetry broken system still captures some features of the observed spectral properties. This indicates that charge-ordering can indeed play a role in determining the properties of the cuprates.

The simplified model considered here has been approximately treated in a mean-field scheme aiming to capture features of well-formed locally ordered stripes in the underdoped cuprates. In this scheme the fermionic quasiparticles do not interact neither among themselves nor with the collective CDW fluctuations. Instead the static symmetry breaking due to charge modulation produces Bragg scattering giving rise to multiple bands and gap opening. As a result the bands arising from the mean-field description are due to δ-like quasiparticle peaks, which obviously do not individually correspond to the real experimental features. Nevertheless, it is worth noting that the multiple Bragg scattering due to incommensuration leads for most k-points to the appearance of multiple quasiparticle peaks (the shadow bands, see Figs. 2, 5, and 7). It is quite natural that the broadening arising from the scattering between quasiparticles and the scattering between quasiparticles and collective modes will mix these peaks thus producing the broad features commonly detected in photoemission experiments. Still we believe that our analysis provides the location and relative position of the spectral features.

We considered one-dimensional charge modulations along the (1,0) and/or (0,1) as well as a two-dimensional eggbox-like texture. The one-dimensional solutions could account for some enhancement of the van Hove singularities, but do not seem particularly successful in describing the appearance of a pseudogap near the M and $\bar{M}$ points. On the other hand the eggbox case turns out to be particularly appealing. The main findings are that the 2-d eggbox CDW scattering might account both for a flattening of the band dispersion in the $\Gamma \rightarrow M$ and $\Gamma \rightarrow \bar{M}$ directions and for the arising of a leading-edge gap around the $M, \bar{M}$ points leaving finite portions of the Fermi surface gapless. As discussed in the introduction, this latter quite unusual and non BCS-like behavior of the gap has indeed been observed [28] and suggests that the charge fluctuations in the particle-hole channel could substantially participate to the spectral features around the $M, \bar{M}$ points. In this regards our finding supports the idea that the scattering induced by a charge ordered superstructure works in many aspects in the same direction than mechanisms involving incoherent pairing correlations (possibly cooperating with magnetic scattering [34]). On the other hand, we also found that a disordering of the eggbox structures "washes out" the weak low-energy features and brings about the disappearance of the leading-edge gap due to charge scattering,

but preserves the feature of Fermi surface only formed by disconnected arcs. In this last situation, the pseudogap will only appear as a (robust) suppression of the spectral weight, which is shifted at higher binding energies.

The overall success of the eggbox CDW scattering in reproducing some highly non-trivial features of the single-particle spectra of the underdoped cuprates suggests that a dynamical charge pseudo-ordering is a relevant aspect of the physics of these materials.

G.S. acknowledges financial support from the Deutsche Forschungsgemeinschaft as well as hospitality and support from the Dipartimento di Fisica of Università di Roma "La Sapienza" where part of this work was carried out. This work was partially supported by INFM-PRA (1996).

References

1. C. Castellani, C. Di Castro, M. Grilli, Phys. Rev. Lett. **75**, 4650 (1995).
2. V.J. Emery, S.A. Kivelson, O. Zachar, Phys. Rev. B **56**, 6120 (1997).
3. S.-W. Cheong *et al.*, Phys. Rev. Lett. **67**, 1791 (1991).
4. T.E. Mason, G. Aeppli, H.A. Mook, Phys. Rev. Lett. **65**, 2466 (1990).
5. T.R. Thurston *et al.*, Phys. Rev. B **46**, 9128 (1992).
6. H.A. Mook, Pengcheng Dai, S.M. Hayden, G. Aeppli, T.G. Perring, F. Dogan, Nature **395**, 580 (1998).
7. H.A. Mook, F. Dogan, B.C. Chakoumakos, `cond-mat/9811100`.
8. J.M. Tranquada, J.D. Axe, N. Ichikawa, A.R. Moodenbaugh, Y. Nakamura, S. Uchida, Nature (London) **375**, 561 (1995).
9. H.A. Mook, *Proceedings of the Conference on High-Temperature Superconductivity and Related Topics (HTS99)*, to be published by the AIP (1999).
10. V.J. Emery, S.A. Kivelson, *Proceedings of the Workshop on Phase Separation in Cuprate Superconductors, Erice, Italy, 6-12 May 1992*, edited by K.A. Müller, G. Benedek (World Scientific, 1992); V.J. Emery, S.A. Kivelson, Physica C **209**, 597 (1993); U. Löw, V.J. Emery, K. Fabricius, S.A. Kivelson, Phys. Rev. Lett. **72**, 1918 (1994).
11. The reason why phase separation nevertheless is experimentally observed in the La_2CuO_{4+y} oxides is that the negatively charged oxygen ions are sufficiently mobile in these materials, thus screening the positive holes and compensating the charge unbalance.
12. F. Becca, M. Tarquini, M. Grilli, C. Di Castro, Phys. Rev. B **54**, (1996).
13. A. Bianconi, Solid St. Commun. **89**, 933 (1994).
14. Concerning the physics of a spin QCP in the cuprates, see S. Sachdev, J. Ye, Phys. Rev. Lett. **69**, 2411 (1992). For an alternative proposal related to a charge-transfer instability, see C.M. Varma, Phys. Rev. Lett. **75**, 898 (1995).
15. A. Perali, C. Castellani, C. Di Castro, M. Grilli, Phys. Rev. B **54**, 16216 (1996).
16. C. Castellani, C. Di Castro, M. Grilli, Z. Phys. B **103**, 137 (1997).
17. C. Castellani, C. Di Castro, M. Grilli, J. Phys. Chem. Solids **59**, 1694 (1998).
18. For a review on photoemission experiments in high temperature superconductors see, *e.g.*, Z.-X. Shen, D.S. Dessau, Phys. Rep. **253**, 1 (1995).
19. M. Randeria, J.-C. Campuzano, `cond-mat/9709107`.
20. D.S. Dessau, Z.-X. Shen, D.M. King, D.S. Marshall, L.W. Lombardo, P.H. Dickinson, A.G. Loeser, J. Di Carlo, C.-H. Park, A. Kapitulnik, W.E. Spicer, Phys. Rev. Lett. **71**, 2781 (1993).
21. K. Gofron, J.C. Campuzano, A.A. Abrikosov, M. Lindroos, A. Bansil, H. Ding, D. Koelling, B. Dabrowski, Phys. Rev. Lett. **73**, 3302 (1994).
22. M.I. Salkola, V.J. Emery, S.A. Kivelson, J. Supercond. **9**, 401 (1996).
23. D.S. Marshall, D.S. Dessau, A.G. Loeser, C.-H. Park, A.Y. Matsuura, J.N. Eckstein, I. Bozovic, P. Fournier, A. Kapitulnik, W.E. Spicer, Z.-X. Shen, Phys. Rev. Lett. **76**, 4841 (1996).
24. H. Ding, T. Yokoya, J.C. Campuzano, T. Takahashi, M. Randeria, M.R. Norman, T. Mochiku, K. Kadowaki, J. Giapintzakis, Nature **382**, 51 (1996).
25. J.M. Harris, P.J. White, Z.-X. Shen, H. Ikeda, R. Yoshizaki, H. Eisaki, S. Uchida, W.D. Si, J.W. Xiong, Z.-X. Zhao, D.S. Dessau, Phys. Rev. Lett. **79**, 143 (1997).
26. N.L. Saini, J. Avila, A. Bianconi, A. Lanzara, M.C. Asensio, S. Tajima, G.D. Gu, N. Koshizuka, Phys. Rev. Lett. **79**, 3467 (1997).
27. M. Randeria, `cond-mat/9710223`.
28. M.R. Norman, H. Ding, M. Randeria, J.C. Campuzano, T. Yokoya, T. Takeuchi, T. Takahashi, T. Mochiku, K. Kadowaki, P. Guptasarma, D.G. Hinks, Nature **392**, 157 (1998).
29. J. Ranninger, J.-M. Robin, M. Eschrig, Phys. Rev. Lett. **74**, 4027 (1995); J. Ranninger, J.-M. Robin, Phys. Rev. B **56**, 8330 (1997).
30. V.B. Geshkenbein, L.B. Ioffe, A.I. Larkin, Phys. Rev. B **55**, 3173 (1997).
31. A.V. Chubukov, D. Pines, B.P. Stojković, J. Phys.-Cond. Matter **8**, 10017 (1996); J. Schmalian, D. Pines, B. Stojković, Phys. Rev. Lett. **80**, 3839 (1998).
32. A.V. Chubukov, D.K. Morr, K. Shakhnovich, Philos. Mag. B **74**, 563 (1996); A.V. Chubukov, D.K. Morr, Phys. Rev. Lett. **81**, 4716 (1998); A.V. Chubukov, J. Schmalian, Phys. Rev. B **57**, 11085 (1997); A.V. Chubukov, Europhys. Lett. **44**, 655 (1998).
33. Z.-X. Shen, J.R. Schrieffer, Phys. Rev. Lett. **78**, 1771 (1997).
34. S. Caprara, M. Sulpizi, A. Bianconi, C. Di Castro, M. Grilli, Phys. Rev. B **59**, 14980 (1999).
35. C. Panagopoulos, T. Xiang, Phys. Rev. Lett. **81**, 2336 (1998).
36. S.E. Barnes, J. Phys. F **6**, 1375 (1976); P. Coleman, Phys. Rev. B **29**, 3035 (1984).
37. N. Read, D.M. Newns, J. Phys. C **16**, 3273 (1983); N. Read, J. Phys. C **18**, 2651 (1985).
38. The occurence of the CDW instability in the present effective model is in good qualitative and quantitative agreement with the instability found in [1,12], where the scattering amplitude of the model equation (1) has been calculated systematically up to order $1/N$ in the spin degeneracy N.